LAWRENCE
LIVERMORE
NATIONAL
LABORATORY

LLNL-CONF-654794

Models of SOL Transport and Their Relation to Scaling of the Divertor Heat Flux Width in DIII-D

M. A. Makowski, C. J. Lasnier, A. W. Leonard, T. H. Osborne, M. Umansky, J. D. Elder, J. H. Nichols, P. C. Stangeby

May 22, 2014

21st International Conference on Plasma Surface Interactions 2014
Kanazawa Ishikawa, Japan
May 26, 2014 through May 30, 2014

Disclaimer

LLNL-CONF-654794 **Paper I-2**

Models of SOL Transport and Their Relation to Scaling of the Divertor Heat Flux Width in DIII-D*

M.A. Makowski[1], C.J. Lasnier[1], A.W. Leonard[2], T.H. Osborne[2],

M. Umansky[1], J.D. Elder[3], J.H. Nichols[4], and P.C. Stangeby[3]

[1]*Lawrence Livermore National Laboratory, Livermore, California 94550, USA.*

[2]*General Atomics, P.O. Box 85608, San Diego, California 92186-5608, USA.*

[3]*University of Toronto Institute for Aerospace Studies, Toronto M3H 5T6, Canada.*

[4]*Princeton Plasma Physics Laboratory, Princeton, New Jersey, USA*

Abstract

Strong support for the critical pressure gradient model for the heat flux width has been obtained, in that the measured separatrix pressure gradient lies below and scales similarly to the pressure gradient limit obtained from the ideal, infinite-n stability codes, BALOO and 2DX, in all cases that have been examined. Predictions of a heuristic drift model for the heat flux width are also in qualitative agreement with the measurements. These results have been obtained using an improved high rep-rate and higher edge resolution Thomson scattering system on DIII-D to measure the upstream electron temperature and density profiles. In order to compare theory and experiment, profiles of density, temperature, and pressure for both electrons and ions are needed as well values of these quantitities at the

separatrix. A simple method to identify a proxy for the separatrix has been developed to do so.

PACS:
JNM Keywords:
PSI-19 Keywords: DIII-D, Divertor, Edge Modeling, Power Deposition
**Corresponding and presenting author address: General Atomics, P.O. Box 85608, San Diego, CA 92186-5608*
Corresponding and presenting author email: makowski1@llnl.gov

1. Introduction

The divertor heat flux footprint width, λ_q, is an important physical and engineering parameter of fusion plasmas as it characterizes the region of peak power deposition on the plasma facing divertor target. Recently, progress has been made in the study of the heat flux width with the establishment of a scaling law applicable to both carbon and metal wall devices [1,2]. The basis for the scaling law, developed for an attached, non-dissipative conditions, is a multi-machine, international database that spans a wide range in multiple physics and engineering parameters. The essential finding is that the heat flux width scales as $\sim 1/B_p$, or equivalently as $\sim 1/I_p$, where B_p is the poloidal magnetic field at the outer midplane and I_p is the plasma current. Significantly, the scaling law for the heat flux width is independent of machine size and only weakly depends on other paramters. When the scaling law is applied to ITER, a heat flux width of ~ 1 mm results, significantly lower than the initially projected width of ~ 5 mm [3]. If this result holds, the amount of dissipation in the SOL will need to increase, which will limit the core plasma operational space [4]. To substantiate this possibility, a physical basis for the scaling law is needed to determine whether ITER and other future devices will operate in a regime for which the scaling law is applicable. This work also extends the scaling to higher density by characterizing upstream profiles in detached conditions, the regime of most interest for ITER.

Many models have been developed for the heat flux width but two general classes are of particular interest. The first is that of critical gradient models. In this case, an edge MHD instability (kinetic ballooning mode (KBM) or resistive ballooning mode (RBM))

becomes unstable and grows rapidly, inducing turbulence. At some point the turbulence causes sufficient transport to modify the pressure profile, which affects the drive for the instability (through the pressure gradient) and inhibits further growth of the mode. This has the effect of locking the pressure profile to the critical gradient for the MHD instablity. Thus a "critical" pressure gradient is established. The heat flux width is then thought to be set by the separatrix pressure gradient scale length.

Stability of the KBM is difficult to compute, so the ideal ballooning mode (IBM) is used as a proxy. The IBM should have a higher stability threshold. As a consequence, it is expected that the measured separatrix pressure gradient should be bounded above by the critical pressure gradient calculated from the ideal ballooning code BALOO and by the more general 2DX code. This is indeed what is observed.

The heuristic drift model posits that grad(B) and curv(B) drifts transport particles from the core to the SOL. Anomolous thermal transport provides the heat carried by the particles. Within the SOL, flows either return the particles back to the core or carry them, at half the sound speed, to the divertor target. A consequence of this model is that the heat flux width should scale as the ion poloidal gyroradius, and thus inverserly with the plasma current, which is also consistent with the empirical scaling law.

In order to compare theory and experiment, profiles of density, temperature, and pressure for both electrons and ions are needed as well as values of these quantitities at the separatrix. Profile analysis is discussed in Section 2, which also includes a discussion of selecting a proxy for the separatrix. Sections 3 discusses the scaling of the heat flux density, while Section 4 evaluates the two models in light of the data. Finally, a summary and conclusion are contained in Section 5.

2. Profile Analysis

Highly resolved upstream profiles of electron density and temperature are routinely obtained on DIII-D using an upgraded Thomson scattering system [5]. Upon detailed analysis it was found that the n_e and T_e profiles are very nearly linear in both the pedestal and SOL and thus are extremely well fit by a hyperbola that is asymptotic to the linear portions of the profile in these two regions. Figure 1 shows a hyperbola (solid blue line) fit to the electron temperature data (red dots). The intersection of the hyperbola asymptotes (dashed green lines) is the point of maximum curvature and corresonds to the inferred separatrix. The local (restricted to the vicinity of the separatrix) hyperbola-fits more accurately model the data than the more commonly used tanh-fits [6], which include data from the top of the pedestal. This difference is important in that although very similar values for $n_{e,sep}$ and $T_{e,sep}$ are obtained from both fits (once a separatrix location has been chosen), the gradients (and thus gradient scale lengths) can differ greatly.

A consistent means of identifying a proxy for the separatrix is necessary to make meaningful comparisons with theory and expose underlying trends in the data. A large number of methods of identifying such a proxy have been examined [7]. One result of this study is that the point of maximum curvature of the hyperbola fit to the electron temperature data is a robust method to define a proxy for the separatrix (see Fig. 1). The method is called robust because, in a majority of cases the fit converges, the resulting separatrix profile values are physically sensible, and clear trends emerge when parameter scans are analyzed. Similar trends are observed with many of the other proxy methods, but they are generally much noisier.

Profile data were obtained under steady-state conditions in an ELMing H-mode, beam heated discharge and with both an attached and detatched outer divertor. The analysis interval, typically 1-2 s in length, contained ~ 50-100 individual Thomson profiles that were combined to form composite profiles. Only Thomson scattering data falling in the last 20-50% of the ELM cycle was used to form the profiles. No difference was found when the same shot was analyzed using either the last 20% or last 50% of the ELM cycle. This is consistent with the fact that the pedestal first forms near the separatrix and grows inward during the ELM cycle. The base of the pedestal, which is formed earliest in time, does not evolve during the later portion of the ELM cycle [8] and is constant over the last 50% of the ELM cycle.

In order to obtain the total pressure the contribution from the ions must be included. The ion pressure and pressure gradient are given by

$$P_i = n_i T_i \approx f_{dil} n_e T_i \qquad (1a)$$

$$\nabla P_i \approx f_{dil} \nabla n_e T_i = f_{dil} \left(n_e \nabla T_i + T_i \nabla n_e \right) \qquad (1b)$$

where f_{dil} is the ion dilution factor defined by

$$f_{dil} = \frac{1}{1 + f_C \left(\bar{Z}_C - 1 \right)} \qquad (2a)$$

$$f_C = \frac{n_C}{n_D + n_C} \qquad (2b)$$

and where f_C (= 0.05) is the carbon impurity fraction (obtained from CER measurements of the fully stripped carbon density fraction at the top of the pedestal and extrapolated to the separatrix), n_C is the carbon density, n_D is the deuteron density, and $\bar{Z}_C$ (= 5) is the mean charge state of carbon. A value of $f_{dil} \sim 0.83$ has been used in the following.

The resolution of the ion CER measurements is much coarser than that of the electrons, so only the data closest to the separatrix is used. Generally, this means only the data from 2-3 edge channels is used to define a line from which the separatrix values of T_i and P_i are obtained. The slope of the line is used to obtain the corresponding gradients and gradient scale lengths. Figure 2 shows the ion temperature profile obtained from charge exchange recombination measurements on carbon.

Using the fits, it is a straightforward task to calculate the pressure gradient as well as the gradient scale length of the various profiles at the inferred location of the separatrix through

$$L_u = \left(\frac{1}{u} \frac{du}{dR} \right)^{-1} \quad . \tag{3}$$

Analysis of the edge profiles in both attached and detached states reveals that the upstream conditions trend similarly and do not appreciably change in transitioning from one regime to another. This is shown in in Fig. 3, which plots n_e, T_e, T_i, P_e, P_i, and P_{tot} as a function of the injected power at two values of the Greenwald fraction corresponding to attached (red circles, $f_{GW} = 0.5$) and detached (blue squares, $f_{GW} = 0.65$) conditions. Within the error of the measurements, the values and trends are very similar.

3. Scaling of the Heat Flux Width with Density

The heat flux width database has been extended with density scans at three different injected power levels as shown in Fig. 4. The measurements are show in solid symbols. The attached divertor results are consistent with the multi-machine empirical scaling law [1] in that there is a very weak dependence of the measured heat flux width, λ_q, on both density and injected power.

There is a clear difference in λ_q between attached and detached (yellow shaded region) divertor conditions, with the heat flux width increasing by a factor of 2 or more when the divertor is detached. Also shown is the conduction limited heat flux width, $\lambda_{q,cond} = 2L_{T_e}/7$, (open symbols), where L_{T_e} is the electron temperature gradient scale length. A linear fit shows that $\lambda_{q,cond}$ does not show a break between attached and detached divertor states as does the measured heat flux width. This suggests that the upstream SOL is independent of the divertor condition.

4. Comparison with models

Analytic calculations, as well as massively parallel gyrofluid simulations, have shown that the critical gradient that triggers the onset of the kinetic ballooning mode (KBM) is close to the critical gradient for the ideal MHD ballooning mode (IBM), with the kinetic corrections having a slight destabilizing effect [9,10] for the KBM, thus making the IBM stability limit an upper bound for that of the KBM. In this study, IBM stability is used as a proxy for KBM stability in order to preserve computational tractability. The BALOO code [11] calculates the IBM-critical pressure gradient at each normalized flux surface in a given magnetic equilibrium, out to $\psi_N = 0.998$. Magnetic equilibria are reconstructed from data by EFIT run in "kinetic" mode, which first calculates a Sauter bootstrap current profile [12] from the measured pressure profile, and then solves for an equilibrium that is consistent with the edge current profile, the measured pressure profile, and an extensive set of magnetic measurements [13]. Since the IBM-critical pressure gradient profile calculated by BALOO is roughly linear from $\psi_N = 0.99$ to $\psi_N = 0.998$, a linear fit in this region is used to extrapolate the boundary incrementally to $\psi_N = 1$ in order to provide an estimate of the KBM-critical pressure gradient at the separatrix. It is expected that kinetic

and resistive effects will lower the stability boundary, but rigorously quantifying these effects has yet to be done because of difficulty of these computations. However the 2DX code [14] now under development, offers a means of doing so.

Frames a-c of Fig. 5 show a comparison of the ideal ballooning mode pressure gradient limit obtained from the BALOO code (open symbols) and the measure total pressure gradient (solid symbols) as a function of normalized density for three different injected power levels. The BALOO pressure gradient limit lies above the measured pressure gradient. This is the expected result if the measured pressure gradient is actually set by the KBM instability with its lower stabiility threshold. In addition, there is a roll-over of the measured pressure gradient at high normalized density, which is attributed to resistive effects that are not included in the BALOO code.

Frames d-f of Fig. 5 show bar charts depicting the contributions to the total measured pressure gradient data of frames a-c from the $n_e \nabla T_e$ (cyan), $T_e \nabla n_e$ (blue), $n_i \nabla T_i$ (green), and $T_i \nabla n_i$ (red) terms as a function of normalized density for three different injected power levels. The contribution from the $T_i \nabla n_i$ term is the largest, accounting for about 45% of the total pressure gradient. Each of the remaining terms accounts for approximately 20% of the total pressure gradient. This points to the importance of having accurate ion temperature measurements.

The BALOO results are corroborated by the 2DX code which solves a generalized linear eignevalue problem for the IBM for a specified toroidal mode number, n, in full 2D geometry with an x-point. The stability limit is obtained by starting with the equilibrium used for the BALOO calculations and increasing the pressure profile by a scale factor. The point at which the mode growth rate, γ, exceeds $\omega_A / 2$, where ω_A is the Alven

frequency, is taken as the stability boundary. Figure 6 plots the normalized growth rate as a function of the pressure scaling factor for several toroidal mode numbers. Instability onset occurs for scale factors in the range of 1.3 – 2.0, indicating that the initial equilibrium (pressure scaling factor = 1) is marginally stable. Figure 7 shows a comparison of BALOO and 2DX calculations for a plasma current scan which has a significant variation in pressure gradient. The measured pressure gradient is depicted by the solid blue circles, the critical pressure gradient obtained from the BALOO code is indicated by the open squares, and the stability boundary obtained from the 2DX code is depicted by the shaded gray region. The agreement between the codes is excellent. In addition, 2DX yields an eigenfunction, which for all the points in the current scan, was just inside the separatrix. The mode exhibit the typical ballooning structure as it is confined to the low field side, peaks at the outer mid-plane, and does not reach the x-point.

An MHD heat flux width is expected to scale with $\beta_{p,sep}$, the separatrix poloidal beta at the outer mid-plane, which gives rise to an effective heat flux width

$$\lambda_{q,balloon} = const \cdot a\beta_{p,sep} \tag{4}$$

where a is the minor radius. Figure 8 plots the measured heat flux width, λ_q , versus $\beta_{p,sep}$. The majority of the data points are clustered in the lower left-hand corner of the plot. There are insufficient higher $\beta_{p,sep}$ points to firmly support a trend, although a trend with $\beta_{p,sep}$ does not appear to be ruled out.

Alternatively, a heuristic drift model has been proposed [14,15] which reproduces many of the observed trends and scalings captured in the multi-machine database of heat

flux widths. Using the highly resolved profile measurements, more direct tests of the model may be made. The model predicts a heat flux width given by [15, Eq (1)]

$$\lambda_{q,hd} = \frac{4a}{eB_p R}\left(\frac{\bar{A} m_p T_{sep}}{1+\bar{Z}}\right)^{1/2} f_{geom} \qquad (5)$$

This is a primal relation upon which the rest of the theory depends. Figure 9 plots the measured heat flux width, λ_q, versus $\sqrt{T_e}/B_{p,sep}$, the only quantities in Eq. (5) that actually vary in the scans that have been made. Once again, the data points cluster in the lower left-hand corner of the plot, and once again no definitive trend is evident, although a scaling with $\sqrt{T_e}/B_{p,sep}$ is not ruled out.

Figures 8 and 9 are very similar in their structure, a fact that makes it difficult to cleanly distinguish the dependencies of one model from the other.

5. Conclusions and Summary

An upgrade to the Thomson scattering system [5] routinely yields highly resolved measurements of the n_e and T_e profiles. The standard tanh-fit [6] has been found to deviate slightly from the data in the vicinity of the separatrix, resulting in inaccurate values and gradients at the location of the separatrix. Local fits are used instead, yielding more faithful fits to the data and allowing detailed comparison of the measurements with theoretical edge models.

For the edge models considered in this paper, the location of the separatrix is needed. Examination of multiple methods to identify the separatrix leads to the conclusion that this cannot be accomplished to better than about +/- 2 mm which is insufficient to extract meaningful trends from the data as profiles gradients are exceedingly steep in this region. Therefore a consistent means of identifying a proxy for the separatrix has been developed

using the local fits. For results presented above the point of maximum curvature of a hyperbola has been used as a proxy for the separatrix. Using this method, very clear trends have been extracted from the various parameter scans that have been made. It is found that there is essentially no difference in the separatrix values and gradients between attached and detached states.

Good suport for the critical ballooning pressure gradient model for the heat flux width has been obtained. In all cases examined, the measured pressure gradient lies below the ideal ballooning mode stability limit and scales similarly to the measured pressure gradient. The fact that the measured pressure gradient lies below the IBM pressure gradient limit is consistent with the IBM being a proxy for the kinetic ballooning mode. The KBM is thought to be the physically limiting instablity, as it is destabilized at a lower pressure gradient. Also, resistive effects appear to be present at the highest normalized pressures, as the measured separatrix pressure gradient decreases in this regime.

However, when measurements are compared to the expected scalings for the heat flux width, the results are less compelling. For both the critical ballooning mode and heuristic drift models, the available data clusters in a single region or parameter space and has insufficient range to firmly a establish a clear trend. The similarity of the predictions of the two models also makes its difficult to differentiate them experimentally.

A number of uncertainties remain, particularly in connection with the ions. The dilution factor is uncertain, as there are no direct measurements of either f_C or $\bar{Z}_C$. Also, the main ion temperature is inferred through the measurement of the carbon temperature. This is known to be accurate in the core where the different ionic species have

equilibrated, but may not be as good an approximation near the separatrix where the temperature is lower and multiple carbon species simultaneously exist. However, the values used should be representative and the result is not highly sensitive to the choice of these parameters. Also, while the stability calculation serves as a good proxy for the critical pressure gradient, it clearly could be improved upon with more realistic separatrix geometry and resistive corrections. The 2DX code will be used to do exactly this.

Acknowledgements

This work was supported by the U.S. Department of Energy under DE-AC52-07NA27344, DE-FC02-04ER54698, and DE-AC02-09CH11466. DIII-D data shown in this paper can be obtained in digital format by following the links at https://fusion.gat.com/global.D3D_DMP.

References

[1] T. Eich, et al., Phys. Rev. Lett. **107** (2011) 215001.

[2] M.A. Makowski, et al. Phys. Plasmas **19** (2012) 056122.

[3] A. Loarte, et al., Nucl. Fusion **47** (2007) S203-S263.

[4] A.S. Kukushkin, et al., J. Nucl. Mat. **438** (2013) S203.

[5] D. Eldon, *et al*., Rev. Sci. Instrum. **83** (2012) 10E343.

[6] G.D. Porter, *et al*, Phys. Plasmas **5** (1998) 1410.

[7] M.A. Makowski, "Relation between the divertor heat width and upstream separatrix profile values in the DIII-D tokamak", submitted for publication to Nucl. Fusion (2014).

[8] R. Groebner, *et al*., Nucl. Fusion **50** (2010) 064002.

[9] B.G. Hong *et al*., Phys. Fluids B **1**, 1589 (1989).

[10] P.B. Snyder *et al*., Phys. Plasmas **8**, 744 (2001).

[11] R.L. Miller, *et al*., Phys. Plasmas **4** (1997) 1062.

[12] O. Sauter, *et al*., Phys. Plasmas **6** (1999) 2834.

[13] T.H. Osborne, *et al*., Journal of Physics: Conference Series **123** (2008) 012016.

[14] D.A. Baver, *et al*., Comp. Physics Comm. **182** (2011) 1610.

[15] R.J. Goldston, Nucl. Fusion **52** (2012) 013009.

Figure Captions

Fig. 1. Hyperbola (solid blue line) fit to electron temperature data (red dots) versus mid-plane major radius. The intersection of the asymptotes (dashed green lines) defines the separatrix (dashed vertical red line).

Fig. 2. Ion temperature profile versus mid-plane major radius, obtained from charge exchange recombination measurements of carbon. A line is fit to pedestal data, usually from 2-3 edge channels, and extrpolated to the separatrix. The slope of the line is used to estimate the separatrix gradient.

Fig. 3. Upstream separatrix values of n_e, T_e, T_i, P_e, P_i, and P_{tot} and their gradients as a function of injected power in attached (red circles; f_{GW} = 0.5) and detached (blue squares; f_{GW} = 0.65) conditions. The magnitude and trends are similar regardless of the divertor state, which decreases between attached and detached states.

Fig. 4. Plots of measured heat flux width, $\lambda_{q,irtv}$, (solid symbols) versus normalized density for three different injected powers. The measured heat flux width increases by more than a factor of 2 when the outer divertor detaches. The conduction limited heat flux width, $\lambda_{q,cond} = 2L_{T_e}/7$, parallels the measurement under attached conditions, but does not increase upon detachment. This suggests that the upstream SOL width and divertor width are decoupled.

Fig. 5. Frames a-c: Comparison of the ideal ballooning mode pressure gradient limit obtained from the BALOO code (open symbols) and the measure total pressure gradient (solid symbols) as a function of normalized density for three different injected power levels. Frames d-f: Bar chart depicting the contributions to the total measured pressure gradient from the $n_e\nabla T_e$ (cyan), $T_e\nabla n_e$ (blue), $n_i\nabla T_i$ (green), and $T_i\nabla n_i$ (red) terms as a

function of normalized density for three different injected power levels. The ion terms account for ~ 65% of the total pressure gradient.

Fig. 6. Plot of growth rate for the ideal ballooning mode obtained from the 2DX code versus pressure scaling factor for three toroidal mode numbers for a representative point on the I_p scan (see Fig. 7.). The mode growth rate increases rapidly as the scaling factor is increased from 1 to 2, indicating that the initial equilibrium (scaling factor = 1) is marginally stable.

Fig. 7. Comparison of the measured total pressure gradient (solid blue circles), that obtained from the BALOO code (open squares), and the instability boundary obtained from the 2DX code (shaded gray region). The two calculations are in excellent agreement with one another and scale closely with the rapidly changing measured pressure gradient.

Fig. 8. Plot of measured heat flux width, λ_q, versus $\beta_{p,sep}$ (proportional to a ballooning heat flux width) for the complete DIII-D data set. No clear correlation is evident, although the data does not rule one out.

Fig. 9. Plot of measured heat flux width λ_q, versus $\sqrt{T_e} / B_{p,sep}$ (proportional to the heuristic drift model heat flux width) for the complete DIII-D data set. No clear correlation is evident, although the data does not rule one out.

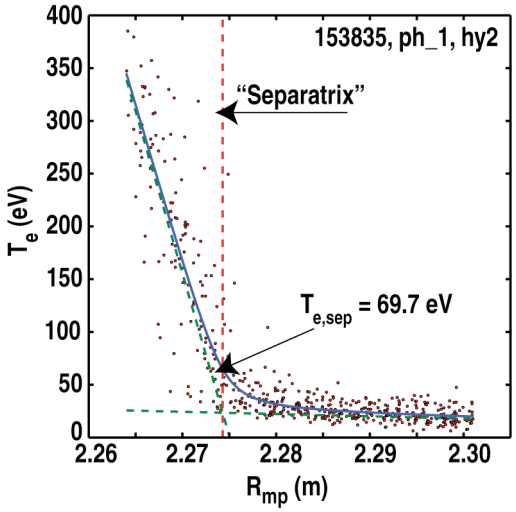
153835, ph_1, hy2
"Separatrix"
$T_{e,sep}$ = 69.7 eV
T_e (eV)
R_{mp} (m)
400
350
300
250
200
150
100
50
0
2.26
2.27
2.28
2.29
2.30

Fig. 1.

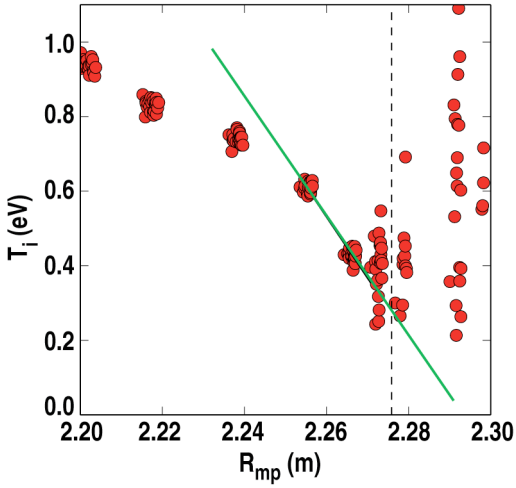

Fig. 2.

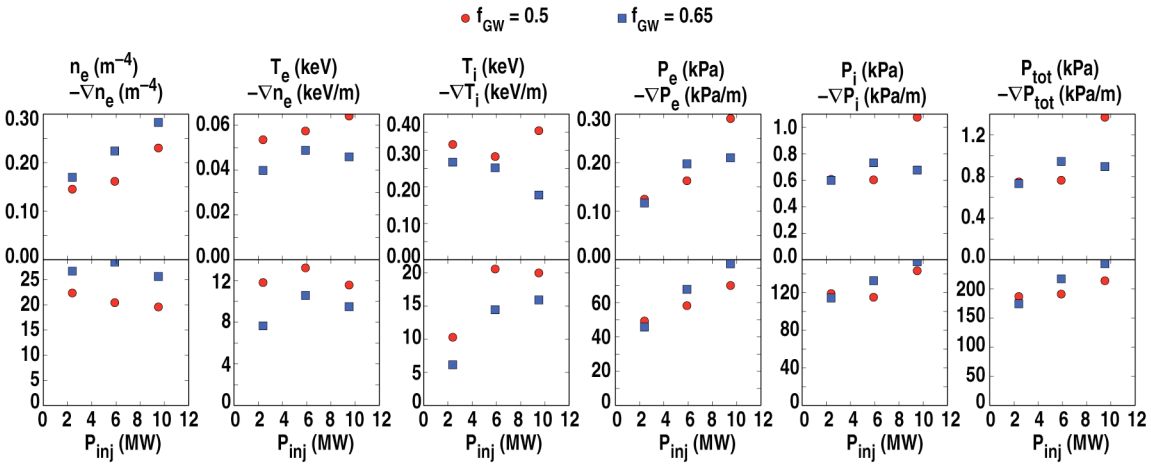
f_GW = 0.5
f_GW = 0.65
n_e (m^-4)
−∇n_e (m^-4)
T_e (keV)
−∇n_e (keV/m)
T_i (keV)
−∇T_i (keV/m)
P_e (kPa)
−∇P_e (kPa/m)
P_i (kPa)
−∇P_i (kPa/m)
P_tot (kPa)
−∇P_tot (kPa/m)
P_inj (MW)

Fig. 3.

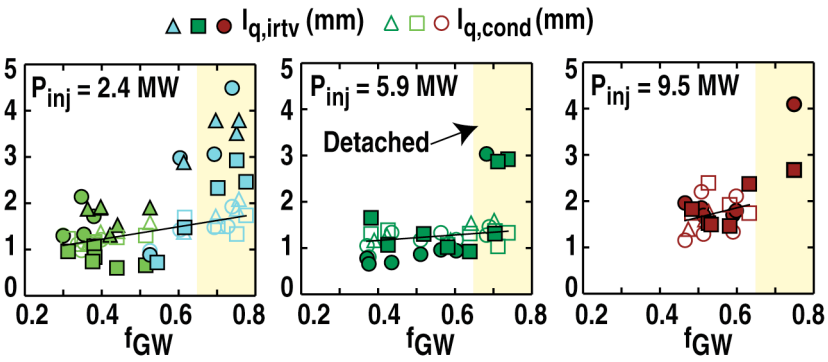
l_q,irtv (mm)
l_q,cond (mm)
P_inj = 2.4 MW
P_inj = 5.9 MW
Detached
P_inj = 9.5 MW
f_GW
f_GW
f_GW

Fig. 4.

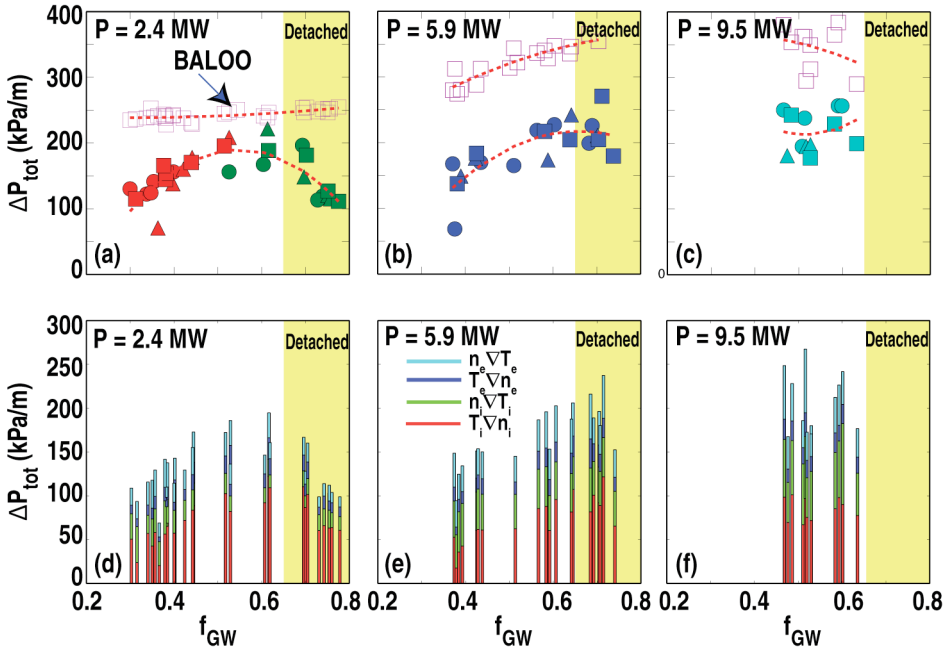
P = 2.4 MW
BALOO
Detached
P = 5.9 MW
Detached
P = 9.5 MW
Detached
(a)
(b)
(c)
ΔP_tot (kPa/m)
P = 2.4 MW
Detached
P = 5.9 MW
Detached
P = 9.5 MW
Detached
n_e∇T_e
T_e∇n_e
n_i∇T_i
T_i∇n_i
(d)
(e)
(f)
f_GW
f_GW
f_GW

Fig. 5.

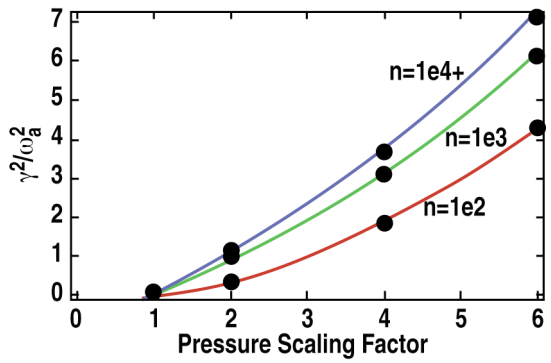
n=1e4+
n=1e3
n=1e2
γ^2/ω_a^2
Pressure Scaling Factor
0
1
2
3
4
5
6
7

Fig. 6.

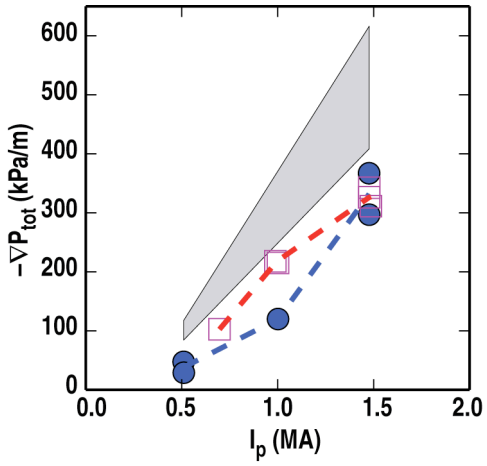

Fig. 7

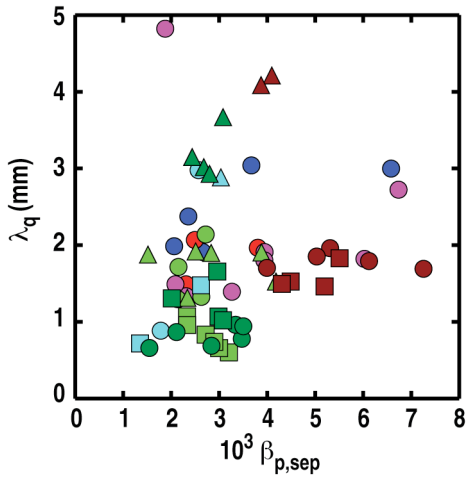

Fig. 8

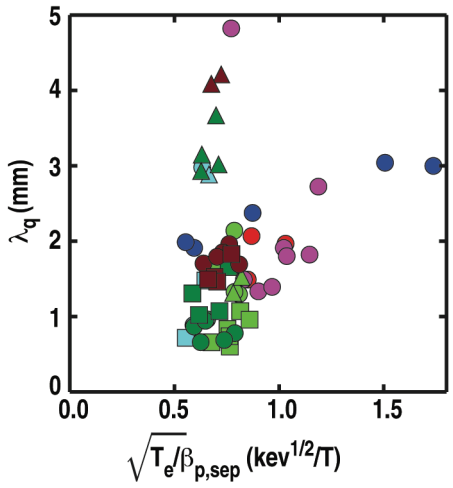

Fig. 9